AIP Journal of Applied Physics

Spatially resolved, excited state densities and neutral and ion temperatures in inductively coupled argon plasmas

G. A. Hebner

Citation: Journal of Applied Physics **80**, 2624 (1996); doi: 10.1063/1.363178
View online: http://dx.doi.org/10.1063/1.363178
View Table of Contents: http://scitation.aip.org/content/aip/journal/jap/80/5?ver=pdfcov
Published by the AIP Publishing

Articles you may be interested in

Negative ion density in inductively coupled chlorine plasmas
J. Vac. Sci. Technol. A **14**, 2158 (1996); 10.1116/1.580040

Measurements of electron temperature, electron density, and neutral density in a radiofrequency inductively coupled plasma
J. Vac. Sci. Technol. A **14**, 144 (1996); 10.1116/1.579911

Power deposition in highdensity inductively coupled plasma tools for semiconductor processing
Phys. Plasmas **2**, 2597 (1995); 10.1063/1.871222

Twodimensional fluid model of high density inductively coupled plasma sources
J. Vac. Sci. Technol. B **12**, 478 (1994); 10.1116/1.587102

Twodimensional modeling of high plasma density inductively coupled sources for materials processing
J. Vac. Sci. Technol. B **12**, 461 (1994); 10.1116/1.587101

High-Voltage Amplifiers
• Voltage Range from ±50V to ±60kV
• Current to 25A

Electrostatic Voltmeters
• Contacting & Non-contacting
• Sensitive to 1mV
• Measure to 20kV

ENABLING RESEARCH AND INNOVATION IN DIELECTRICS, ELECTROSTATICS, MATERIALS, PLASMAS AND PIEZOS

TRek www.trekinc.com

TREK, INC. 190 Walnut Street, Lockport, NY 14094 USA • Toll Free in USA 1-800-FOR-TREK • (t):716-438-7555 • (f):716-201-1804 • sales@trekinc.com

DOCKET ALARM
Find authenticated court documents without watermarks at docketalarm.com.

Spatially resolved, excited state densities and neutral and ion temperatures in inductively coupled argon plasmas

G. A. Hebner[a)]
Sandia National Laboratories, Albuquerque, New Mexico 87185-1423

(Received 12 February 1996; accepted for publication 30 May 1996)

Spatially resolved, line integrated, excited state densities, and neutral and ion temperatures have been measured in inductively coupled argon plasmas. Absorption spectroscopy was used to measure the line integrated density and temperature of the argon $1s_5$, $1s_4$, $1s_3$, and $1s_2$ energy levels. Laser-induced fluorescence was used to confirm the neutral temperatures and to measure argon metastable ion temperatures. For rf powers between 50 and 300 W and pressures of 4–50 mTorr, the line integrated density of the $1s_5$ energy level varied between 1×10^{16} and 2×10^{16} m^{-2}. The densities of the $1s_4$, $1s_3$, and $1s_2$ levels were approximately 4–10 times smaller. In the center of the plasma, the ion and neutral temperatures were identical, between 550 and 1000 K for plasma powers between 30 and 240 W and pressures between 4 and 50 mTorr. The neutral temperature had a maximum in the center of the discharge and decreased towards the edge of the discharge. However, the ion temperature increased to between 3000 and 4000 K at the edge of the discharge. Ion drift velocity in the radial direction was between 1×10^5 and 2×10^5 cm/s at the edge of the plasma. No significant changes in the spatial density distribution or temperature were observed when either a rf bias was applied to the lower electrode or when the stainless-steel lower electrode was covered with a bare silicon wafer. The addition of nitrogen to the argon discharge resulted in the density of the $1s_5$ state decreasing by a factor of 2 and the density of the $1s_4$ state decreasing by a factor of 10. Implications of these measurements on the radial electric fields, radiation trapping, and the energy transport in the plasma are discussed. [S0021-8979(96)02817-4]

I. INTRODUCTION

As integrated circuit dimensions decrease and feature aspect ratios increase, plasma etching becomes more challenging and control of the ion energy and angle striking the wafer surface becomes more critical. The current generation of high-density plasma processing reactors has been developed to address the increasingly stringent industrial requirements for a uniform, high-density source of ion and chemically reactive neutral species over large diameters ($d\geqslant200$ mm) with controllable ion energy at the wafer surface and with reduced contamination.[1] The inductively coupled plasma (ICP) source is one tool that has been developed to satisfy current requirements. In theory, ICP sources can provide independent control of the ion energy at the surface of the wafer, and the bulk plasma parameters such as ion density. The bulk plasma parameters are set by the power and geometry of the inductive antenna while the ion energy is controlled by the bias voltage on the wafer chuck. In practice, there can be a significant overlap of control between the antenna power and wafer bias. An improved understanding of the relevant plasma physics and bias sheath characteristics will aid in improving these tools to meet current and future production requirements.

While radio-frequency inductively coupled discharges are not new, they have only recently been used for semiconductor plasma processing. As a result, recent work has focused on both measurements of fundamental plasma parameters[1–16] and the development of codes[17–25] to improve our understanding of the important physics of ICP sources. In order to understand the fundamental plasma physics mechanisms and to provide data to benchmark codes, many experiments have focused on inductive discharges in argon. Argon has the advantage of a relatively complete set of cross sections, and a minimum of discharge chemistry. Recent experiments in argon ICP systems include characterization of the rf circuit and rf power deposition,[2,10,11] measurements of the electron density, electron energy distribution, temperature and plasma potential using Langmuir probes and microwave interferometry,[2,3–7] spatially resolved electromagnetic fields,[8,9] and optical emission.[15,16] In particular, probe measurements have shown that the electron density is maximum in the center of the discharge.[2] However, the optical emission has been shown to peak in a ring-shaped region that corresponds to the regions of maximum electric field and electron heating.[8,9,15] Measured azimuthal electric fields had a ring shape with a maximum electric field of approximately 4–8 V/cm centered between the center of the coil and the edge.[9] Code results confirm the location and magnitude of the electric field, and also indicate that the location of the maximum electric fields corresponds to the region of greatest power deposition and excitation.[19–24]

Ion energy measurements can be used to provide insight into sheath and presheath characteristics such as potential drop and energy transfer mechanisms such as charge exchange and elastic collisions.[12–14] For example, argon-ion energy measurements at the grounded wafer surface indicated that the peak ion energy in an ICP system is approximately equal to the plasma potential and that the ion energy

Find authenticated court documents without watermarks at docketalarm.com.

angular distributions shows that the transverse argon ion energy at the wafer surface is on the order of 3500–5000 K.[13] In addition to analysis of the ion energy at the surface, laser-induced fluorescence (LIF) is a sensitive, noninvasive, spatially localized probe of the ion energy distribution function (IEDF) in the bulk of the plasma.[26–29] However, due to the thin sheath length in high electron density plasmas, LIF can not be used to probe the ion energy distributions at the wafer surface. Thus, LIF measurements of the bulk plasma IEDF are complimentary to electrostatic measurements of the ion energy distributions obtained through pinholes in the lower electrode surface; LIF provides the IEDF before the sheath and electrostatic probes provide the IEDF after the sheath.

Ion and neutral temperatures can also be determined by analyzing the line shape of the plasma optical emission using a scanning Fabry–Pérot interferometer.[16,30,31] Since the measurement is performed along a line of sight in the plasma, it is difficult to obtain good spatial resolution and to identify Doppler shifts due to species drift.

The objective of this work is to examine the details of the excited state and ion interactions in argon ICP systems. To this end, two different but complementary experimental techniques were employed. First, absorption spectroscopy was utilized to measure the spatially resolved density and temperature of the argon $1s_5$, $1s_4$, $1s_3$ and $1s_2$ (Pashen notation) energy levels. Second, spatially resolved LIF was used to confirm the argon neutral temperatures and measure the metastable argon ion temperature. Separately, these two measurement techniques provide information on fundamental discharge parameters such as species density, species temperature, transverse ion energy, radial electric fields, electron collisional induced mixing, and radiation trapping. When examined together, these experiments provide information on the energy exchange between neutral and ion species, charge exchange and an experimental cross check of the unexpectedly high neutral temperatures. For example, the metastable argon energy levels ($1s_5$ and $1s_3$), and the resonance levels ($1s_4$ and $1s_2$ levels, radiatively coupled to the ground state but radiation trapped) can be important to the discharge physics since they comprise a reservoir of significant energy and density within the plasma. The relative population density in these energy levels provides an indication of the importance of electron collisional quenching and radiation trapping. Since LIF measurements provide information on the ion energy distributions before they are modified in the sheath, they can be used, together with measurements of the ion energy at the surface,[12–14] to provide insight into the energy transfer mechanisms between the charged and uncharged plasma species, to gain information about the effects of collisions in the presheath region on the ion energy distribution, and to benchmark sheath and presheath codes.

Due to the many processes involved, the accurate prediction of the excited state densities, temperatures, and ion energies can be a stringent test of discharge codes. To facilitate code comparisons, this article includes a characterization of the voltage and current in the inductive coil and the bias electrode.

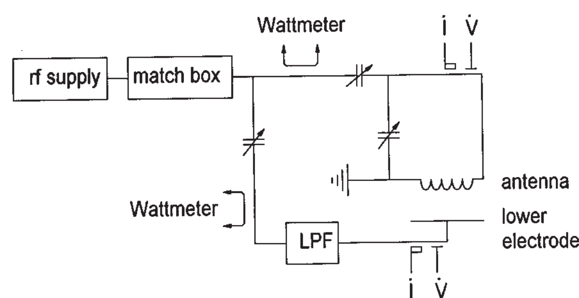

FIG. 1. Schematic of the rf circuit used to power the inductive coil and bias the lower electrode. In most cases the lower electrode was grounded and the bias circuit was disconnected.

II. rf CHARACTERIZATION

The experiments were performed in a Gaseous Electronics Conference (GEC) rf reference reactor that has been modified to include an inductively coupled plasma source.[2,32] Design and construction details of this system have been previously discussed.[2] Briefly, the inductive coil was a five-turn, 11-cm-diam, planar coil constructed from 1/8-in.-diam, oxygen-free high-conductivity (OFHC) copper tubing. The coil was separated from the plasma by a 1-cm-thick quartz window. Distance from the window to the lower electrode was 3.8 cm. The lower electrode can be grounded, or biased with rf or dc voltage. Due to the design of the ICP source, the clear view between the ICP antenna and the lower electrode was approximately 13 cm in the radial dimension and 3.1 cm in the axial dimension. Both the inductive coil and the lower electrode were water cooled.

A schematic of one of the circuits used to supply rf power (13.56 MHz) to the inductive coil and bias power to the lower electrode is shown in Fig. 1. One of the experimental parameters that was investigated in this study was the influence of lower electrode bias. In some cases, the lower electrode was grounded by connecting it to the metal vacuum chamber. When the lower electrode was grounded, the rf supply (ENI ACG-5) was connected directly to the inductive coil matching network and the match box (ENI Matchwork 5) shown in Fig. 1 was not used. The inductive coil circuit consisted of two vacuum variable tuning capacitors, directional wattmeter (Bird 4411), and calibrated Vdot and Idot probes. The details of the inductive system and calibration of the voltage and current probes have been discussed previously.[2]

When the lower electrode was biased with rf power, output from the rf power supply and impedance matching circuit was connected to the inductive coil matching network and the lower electrode bias circuit. A fraction of the output power from the rf source and matching network was supplied to the lower electrode bias circuit using a series variable capacitor. The matching network after the rf supply was found to be necessary to keep the load impedance at the rf generator near 50 Ω as the lower electrode bias power was varied (by changing the series coupling capacitance). A custom low-pass filter was used to isolate the drive system from the harmonics generated by the plasma.[33–35] The cable length between the coupling capacitor and the low-pass filter

DOCKET ALARM
Find authenticated court documents without watermarks at docketalarm.com.

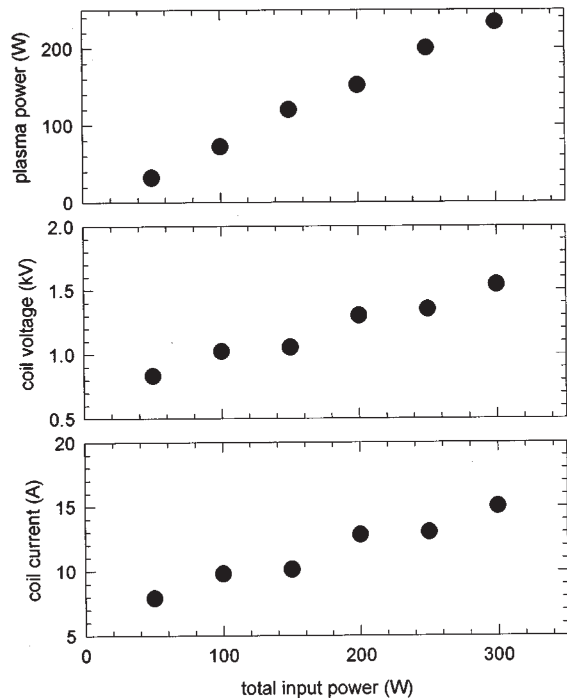

FIG. 2. Power into the plasma, coil voltage, and coil current as functions of total input power (forward power–reflected power). The argon pressure was 10 mTorr and the lower stainless-steel electrode was grounded.

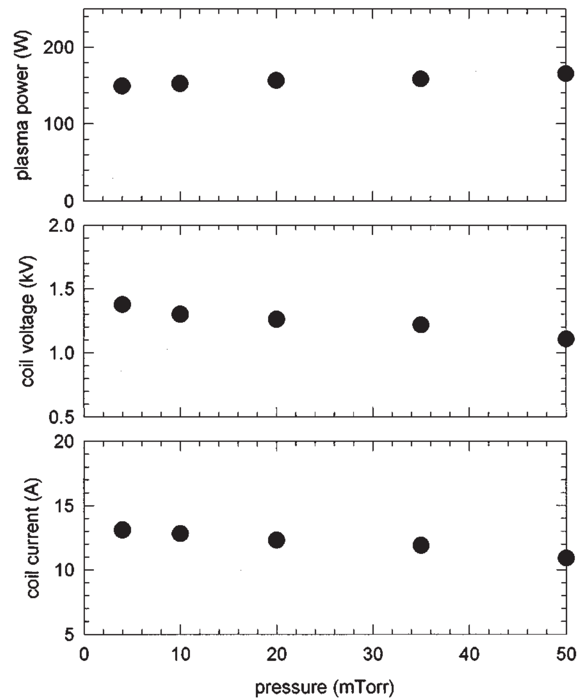

FIG. 3. Power into the plasma, coil voltage, and coil current as functions of argon pressure. The total input power was 200 W and the lower stainless-steel electrode was grounded.

adjusted to match the impedance of the lower electrode bias circuit. Reflected power in the bias circuits was typically 10%–30% of the forward power. Voltage and current at the lower electrode were measured by using calibrated Vdot and Idot probes and an equivalent circuit model to derive the voltage and current at the electrode, similar to the procedure used for parallel-plate rf discharge studies.[32–35]

Voltage and current for the inductive coil are shown in Figs. 2 and 3 as a function of power and pressure respectively. For the data in Fig. 2, the argon pressure was constant at 10 mTorr and for the data in Fig. 3, the total input power was 200 W. In both cases, the lower electrode was grounded. Total input power was the difference between the forward and reflected rf power as measured by the wattmeter. In all cases, the reflected power was less than 2 W. Plasma power is the difference between the total input power minus the power deposited into the coil, calculated from $I^2R/2$. For a typical coil resistance of 0.5 Ω, approximately 80% of the total input power was deposited into the plasma. The reported voltages and currents are zero to peak values.

The rf characteristics of the lower electrode bias circuit are shown in Fig. 4 as functions of the bias power. For these measurements, the total input power into the inductive coil was maintained at 200 W and the pressure was 10 mTorr. Two electrode materials were used, the native stainless steel and a 6-in.-diam silicon wafer placed on top of the stainless-steel electrode (6.5 in. diameter). The wafer was bare silicon, without photoresist or patterning and no attempt was made to remove the native oxide. The intent of the experiment was to investigate the effect of different surface materials on the

creased, the rf voltage, current, and impedance increased, independent of surface material; however, the dc self-bias and phase were different for the two materials. This is likely the result of the different secondary electron generation properties of silicon and stainless steel.

III. EXPERIMENTAL CONFIGURATION

A. Absorption measurements

A schematic of the experimental configuration used to make the two-dimensional absorption measurements is shown in Fig. 5. Output from an argon-ion-laser-pumped ring titanium (Ti)–sapphire laser (Coherent 899-21) was amplitude stabilized (Coherent Noise Eater) and collimated using a 6-in.-diam telescope. Collimation was optimized by using a shear plate. The collimated light was passed through the entire discharge volume and then imaged onto a charge-coupled-device (CCD) camera (Hamamatsu C3140, 512 ×480 pixels) using a second telescope. Spectral bandpass filters (Δλ=10 nm) and neutral density filters (OD=2.5–3.5) were placed in front of the CCD camera to attenuate the laser, discharge emission, and room lights. Spatial resolution in this configuration was less than 0.5 mm. A fraction of the laser output was directed to a wavemeter (Burleigh) and étalon (7.5 GHz free spectral range) to monitor the absolute laser frequency.

To measure the line integrated density, the output wavelength of the Ti–sapphire laser was scanned across the absorption lineshape. Typically, the laser was scanned a total of 6 GHz in 51 discrete steps. The laser was tuned to 801.4,

DOCKET ALARM
Find authenticated court documents without watermarks at docketalarm.com.

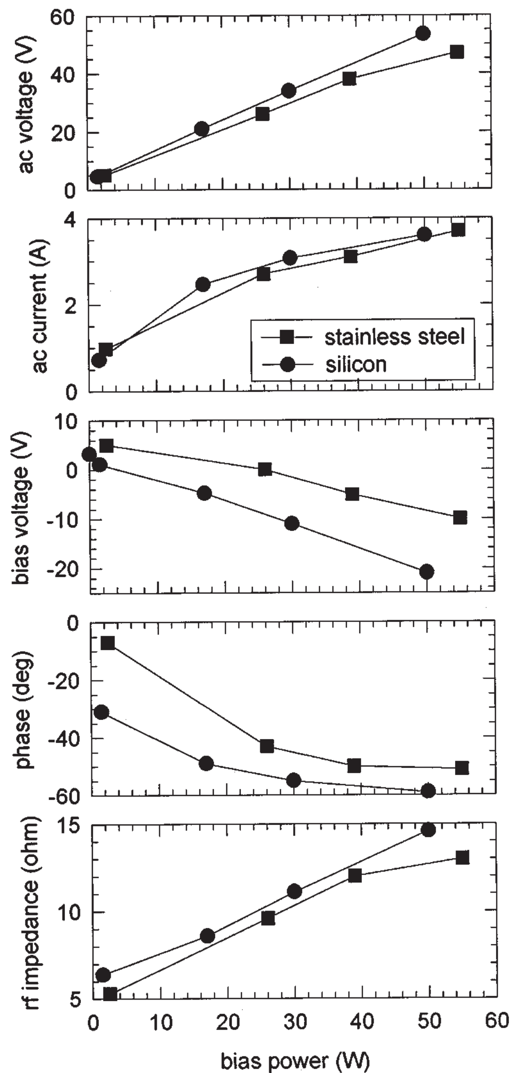

FIG. 4. rf voltage, current, bias voltage, phase, and rf impedance (magnitude) as functions of lower electrode bias power for two electrode materials, stainless steel and silicon. The inductive coil total input power was 200 W and the pressure was 10 mTorr.

$1s_4(1s_4-2p_7)$, $1s_3(1s_3-2p_4)$, and $1s_2(1s_2-2p_2)$ energy levels of neutral argon, respectively. The $1s_5$ and $1s_3$ energy levels are metastable levels while the $1s_4$ and $1s_2$ levels are radiatively coupled to ground. At each laser wavelength, the

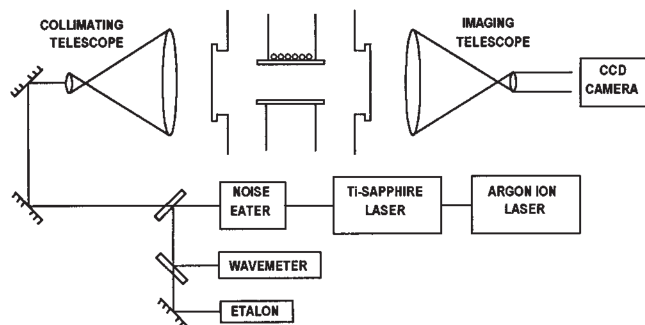

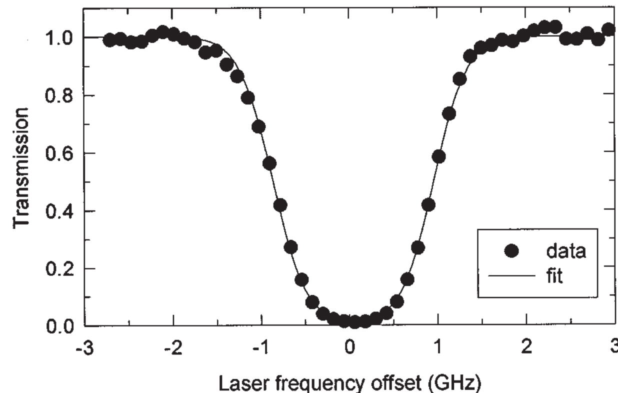

FIG. 6. Example of the 801.4 nm ($1s_5-2p_8$) absorption line shape as scanned by the Ti–sapphire laser and the fit. Total input power was 200 W at 10 mTorr argon. Optimized fit parameters were line-integrated density of 1.97×10^{16} m^{-2}, Doppler width of 1.149 GHz (751 K,) and frequency offset of 48 MHz.

2D CCD image of the transmitted laser light was stored. In addition, the background plasma emission was recorded and subtracted from each laser image before processing. To reduce the data to manageable quantities, the pixels of the CCD camera data were averaged. Typically, pixels in an 8×16 array were averaged. The averaged data was then fit to a Voigt absorption line shape[36] using a computer program. The unknowns in the Voigt line-shape fit were line integrated density, Doppler width, and center frequency. To optimize the line-shape fit, the center frequency determined by the line-shape fitting program was allowed to vary within the uncertainty of the absolute center frequency of the probed transition. The uncertainty in the absolute center frequency (±75 MHz) was related to the frequency uncertainty in the wavemeter and the étalon. Neutral temperatures (K) were determined from the Doppler width. If the energy distribution function is well fit by a Gaussian profile, then temperature is a good parameter to describe the distribution function. As confirmed by the LIF measurements (discussed below), the neutral temperature data were well fit by a Gaussian line shape.

An example of the raw transmission data and optimum fit are shown in Fig. 6 for an absorption measurement on the 801.4 nm argon transition ($1s_5-2p_8$). For these discharge conditions (200 W, 10 mTorr), the absorption on line center was greater than 99% and the line shape was significantly different than a pure Gaussian or Lorentzian. For the data in Fig. 6, the optimum fit parameters returned by the computer algorithm were integrated density of 1.97×10^{16} m^{-2}, Doppler width of 1.149 GHz (751 K), and a small center frequency offset of 48 MHz. In all cases, the absolute frequency offset provided by the computer fitting program was less than 50 MHz. The uncertainty in the line integrated density ($\pm10\%$) and the temperature ($\pm10\%$) is based upon several measurements of the $1s_5$ energy level under nominally identical operating conditions over the course of several months and upon a sensitivity analysis of the line-shape fitting pro-

DOCKET ALARM
Find authenticated court documents without watermarks at docketalarm.com.

DOCKET ALARM

Explore Litigation Insights

Docket Alarm provides insights to develop a more informed litigation strategy and the peace of mind of knowing you're on top of things.

Real-Time Litigation Alerts

Keep your litigation team up-to-date with **real-time alerts** and advanced team management tools built for the enterprise, all while greatly reducing PACER spend.

Our comprehensive service means we can handle Federal, State, and Administrative courts across the country.

Advanced Docket Research

With over 230 million records, Docket Alarm's cloud-native docket research platform finds what other services can't. Coverage includes Federal, State, plus PTAB, TTAB, ITC and NLRB decisions, all in one place.

Identify arguments that have been successful in the past with full text, pinpoint searching. Link to case law cited within any court document via Fastcase.

Analytics At Your Fingertips

Learn what happened the last time a particular judge, opposing counsel or company faced cases similar to yours.

Advanced out-of-the-box PTAB and TTAB analytics are always at your fingertips.

API

Docket Alarm offers a powerful API (application programming interface) to developers that want to integrate case filings into their apps.

LAW FIRMS

Build custom dashboards for your attorneys and clients with live data direct from the court.

Automate many repetitive legal tasks like conflict checks, document management, and marketing.

FINANCIAL INSTITUTIONS

Litigation and bankruptcy checks for companies and debtors.

E-DISCOVERY AND LEGAL VENDORS

Sync your system to PACER to automate legal marketing.

WHAT WILL YOU BUILD? | sales@docketalarm.com | 1-866-77-FASTCASE

fastcase®
Smarter legal research.